

Fast Lithium Ionic Conductivity in Complex Hydride-Sulfide Electrolytes by Double Anions Substitution

Tengfei Zhang, Yifei Shao, Xiang Zhang, Yuqin Huang, Shuai Wang, Wei Zhou, Peng Li,* Guanglin Xia, and Xuebin Yu*

Hydride-based solid-state electrolytes (SSEs) can maintain their stability against Li metal and exhibit high compatibility with a Li metal anode owing to their reducing property and flexible character. However, poor ionic conductivity at room temperature is a major challenge for hydride materials used as SSEs in a lithium ion battery. In this work, a room-temperature fast lithium-ion conductor is explored in response to double anion substitution, (100-*x*) (3LiBH₄-LiI)-*x*P₂S₅ (LLP*x*, 0 ≤ *x* ≤ 50). Among these samples, LLP20 respectively delivers an ionic conductivity up to 3.77 × 10⁻⁴ S cm⁻¹ at 30 °C and 1.0 × 10⁻² S cm⁻¹ at 100 °C, with a stable electrochemical window of 0–5 V. A Li plating/stripping test has been conducted under a current density of 1.0 mA cm⁻², which exhibits an excellent stability even after 1000 h. Moreover, the all solid-state cell exhibits a remarkable electrochemical performance in a wide temperature range including high reversible capacity, good rate capability, and long cycling durability. These outstanding performances present a practical strategy for developing ambient-temperature, fast ionic conductors for all solid-state batteries in near future.

and smart grids.^[1–9] Current liquid electrolytes suffer from low stability and poor compatibility to electrodes, which usually cause nonnegligible safety issues and fast capacity decay.^[10–16] Therefore, substitution of the organic liquid electrolytes by solid-state electrolytes (SSEs) is one of the key challenges to lithium ion battery technology. Extensive efforts have been devoted to developing SSEs with high ionic conductivity, wide electrochemical window, and excellent compatibility. In this respect, various inorganic solid electrolytes, such as, lithium phosphorus oxynitride,^[17,18] perovskite,^[18–21] sodium superionic conductor,^[18,22–24] garnet,^[25–29] sulfide,^[3,12,30–33] halide,^[33,34] and hydride^[35–43] materials, are potential candidates to replace organic liquid electrolytes. Among them, complex hydrides have been widely studied as SSEs in next-generation LIBs since 2007.^[44] LiBH₄ based

SSEs, as typical complex hydrides, exhibit a wide electrochemical window up to 5 V (vs Li/Li⁺), and are compatible to lithium metal anode and sulfur cathode.^[41,43] However, these materials only present a high conductivity of 10⁻³ S cm⁻¹ at more than 120 °C owing to phase transition.^[45]

To enhance the lithium ionic conductivity, several strategies have been implemented such as partial anion substitution and nanoconfinement. The mixed anion effect is a well-known method for improving the ionic conductivity of materials by introduction of a new anion, for example a halide ion (I⁻ or Br⁻),^[46] azide ion (N³⁻),^[18,47] or phosphate (PO₄³⁻),^[48–50] into the original matrix. Doping anion with larger radius allows for inducing ion transport channels and decreasing lithium ion density, and thereby increasing lithium ionic conductivity. Orimo et al. reported that high temperature (HT) phase LiBH₄ can be stabilized at low temperature by partial doping with Li halides (LiX, where X represents Cl, Br, or I). Among the LiBH₄-LiX composites, 3LiBH₄-LiI shows a relatively high ionic conductivity of 2 × 10⁻⁵ S cm⁻¹ at 27 °C.^[38] However, this value is still far from their practical applications as SSEs. More recently, sulfide (P₂S₅) was introduced to hydride system and a high lithium ionic conductivity was reported by Hauback et al.^[51] Structural analysis and characterization suggest that BH₄ and PS₄ groups may belong to the same molecular structure, where [BH₄]⁻ can be partially replaced by [PS₄]³⁻. These studies suggest that partial substitution of [BH₄]⁻ by I⁻ and [PS₄]³⁻ would

1. Introduction


High energy and power densities are the basis for the large-scale application of lithium-ion batteries (LIBs) in the near future, especially in portable electronic devices, electric vehicles,

Dr. T. Zhang, Y. Shao, X. Zhang, Dr. P. Li
Jiangsu Key Laboratory of Electrochemical Energy-Storage Technologies
College of Materials Science and Technology
Nanjing University of Aeronautics and Astronautics
Nanjing 210016, China
E-mail: LPeng@nuaa.edu.cn

Y. Huang, Dr. G. Xia, Prof. X. B. Yu
Department of Materials Science
Fudan University
Shanghai 200433, China
E-mail: yuxuebin@fudan.edu.cn

Dr. S. Wang
Department of Mechanical and Energy Engineering
Southern University of Science and Technology
Shenzhen 518055, China

W. Zhou
Department of Physics
Tianjin University
92 Weijin Road, Nankai District, Tianjin 300072, China

 The ORCID identification number(s) for the author(s) of this article can be found under <https://doi.org/10.1002/smt.202100609>.

DOI: 10.1002/smt.202100609

further stabilize the high temperature phase and thereby obtain high Li^+ conductors.

In this work, we investigated the possibility of double anions substitution and studied a series of pseudo-ternary composite SSEs composed of hydride and sulfide, namely $(100-x)(3\text{LiBH}_4\text{-LiI})\text{-}x\text{P}_2\text{S}_5$ (LLP x , $0 \leq x \leq 50$). Within this system, LLP20 exhibited an ultrahigh lithium ionic conductivity of $\log(\sigma \text{ S}^{-1} \text{ cm}^{-1}) = -4$ at 30°C , with a wide electrochemical window of 0–5 V and favorable mechanical strength and flexibility. Li plating/stripping tests confirmed the electrochemical stability of the interface. The cycling stability and rate performance were investigated through all solid-state batteries at moderate temperature. First-principal calculations revealed that Li ions diffuse in a 1D channel along a and b direction in the LLP20 structure with much lower barrier energy (0.5 eV) than $3\text{LiBH}_4\text{-LiI}$ (0.7 eV) or LiBH_4 (0.9 eV), which is responsible for the superior ion conductivity. These findings provide new insights into the design and development of novel composite hydride-based SSEs for all solid-state lithium ion battery at room temperature.

2. Experimental Section

2.1. Synthesis of $3\text{LiBH}_4\text{-LiI}$

LiBH_4 (95%, Sigma-Aldrich), LiI (99.9%, aladdin), and P_2S_5 (99%, aladdin) were stored in Ar gas-filled glove box (≤ 0.1 ppm O_2 , H_2O) and used as purchased. $3\text{LiBH}_4\text{-LiI}$ was prepared by mechanical milling with molar ratio of 3:1. Then, the composite compound was annealed at 140°C for 2 h in an Ar-filled environment (Figure 1a).

2.2. Synthesis of $(100-x)(3\text{LiBH}_4\text{-LiI})\text{-}x\text{P}_2\text{S}_5$

$(100-x)(3\text{LiBH}_4\text{-LiI})\text{-}x\text{P}_2\text{S}_5$ compound was prepared by mechanical milling from the mixture of $3\text{LiBH}_4\text{-LiI}$ and P_2S_5 . The mixture was hand-milled in an agate mortar for 15 min in the glove box, and further milled via planetary ball-milling (Fritsch, P7) at a rotation rate of 400 rpm for 3 h. Then, the mixture was annealed at 120°C for 2 h in a vacuum environment (Figure 1a).

2.3. Material Characterization

The X-ray diffraction (XRD) measurements were carried out for the as-received samples. Phase identification was measured by using a PANalytical Empyrean Multipurpose X-ray diffractometers with a copper $K\alpha$ line ($\lambda = 1.540598 \text{ \AA}$). Samples for XRD analysis were prepared in a glove box and sealed with Kapton films. Characterizations of the vibrational states were performed by Raman spectroscopy (Nicolet Almega-HD, Thermo Scientific) using a dedicated cell without moisture and air exposure.

2.4. Electrochemical Measurements

The ionic conductivities were measured by electrochemical impedance spectroscopy (EIS, 7 MHz–1 Hz, Biologic VMP 300). The powder samples were pressed into 10 mm diameter pellet of above 1 mm thickness by a uniaxial press in glove box at room temperature. The coin-type cells (CR 2032) were assembled in an argon-filled glove box with lithium metal as the counter and reference electrodes. The electrochemical stability was measured by using cyclic voltammetry (Biologic VMP 300)

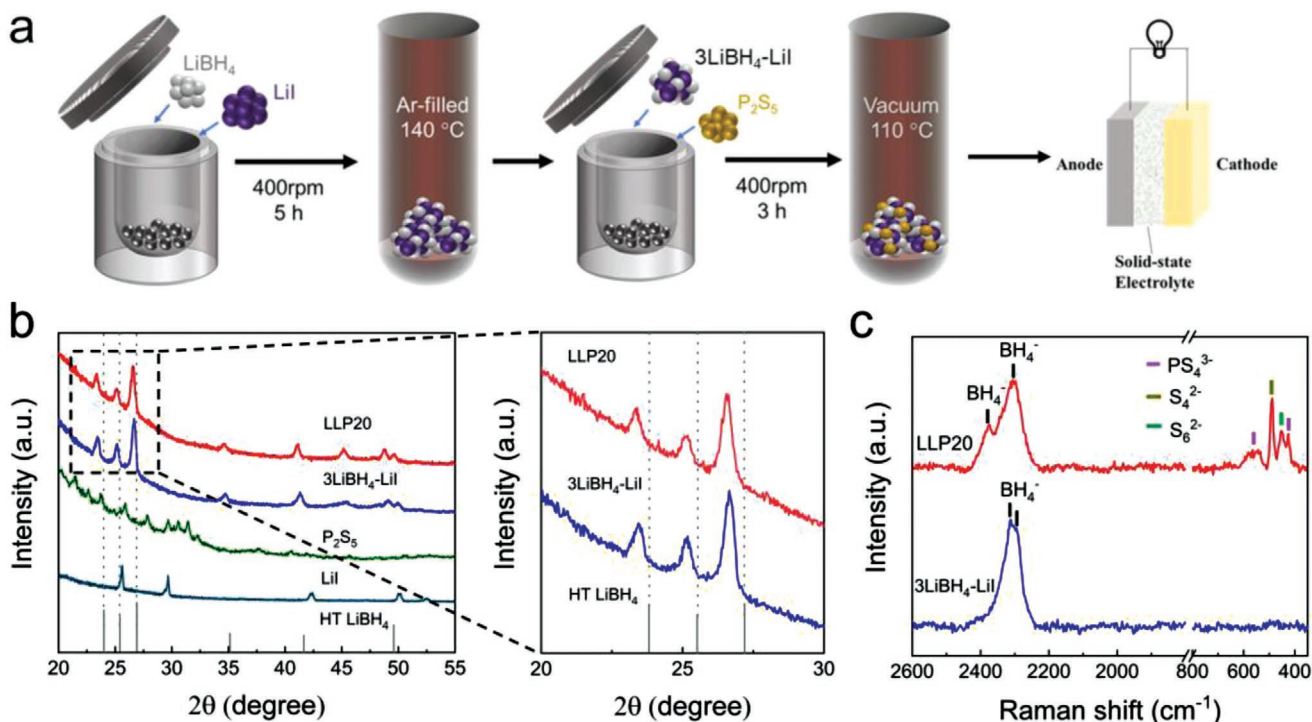


Figure 1. a) Schematic view of the sample synthesis path. b) XRD patterns. c) Raman spectra of $3\text{LiBH}_4\text{-LiI}$ and LLP20.

with a stainless-steel (SUS)/SSE/Li cell in the scan range of -0.2 to 5 V (vs Li/Li⁺). Lithium plating/stripping cycling was evaluated with Li/SSE/Li cells at different current density from 0.2 to 1 mA cm⁻² using a battery tester (LAND, China).

To test the performance of full cells, Li₄Ti₅O₁₂ (LTO) (99.9%, Sigma-Aldrich) and sulfurized pyrolyzed poly(acrylonitrile) (SPAN) were used as working electrode, respectively. Active materials, LLP20 and Ketjen Black (4:5:1 in weight ratio) were milled as cathode. The cells were placed into oil bath and the electrochemical performance of batteries was measured by galvanostatic cycling (Land, China).

3. Results and Discussion

3.1. Materials Synthesis and Characterization

Figure 1a shows the schematic synthesis procedure of LLP_x and the corresponding XRD patterns are shown in Figure 1b. The diffraction peak position of 3LiBH₄-LiI is corresponding to the HT phase of LiBH₄ in agreement with previous report. On the other hand, the addition of P₂S₅ to this system (sample LLP10, LLP20, LLP30) leads to the same Bragg peaks of 3LiBH₄-LiI (Figure S1, Supporting Information), which indicates P₂S₅ as a dopant entering into the structure of 3LiBH₄-LiI. According to XRD pattern analysis (Figure 1b and Table S1, Supporting Information), the lattice spacing of (0 1 1) keeps increasing from 3.266 Å (HT-LiBH₄) and 3.341 Å (3LiBH₄-LiI) to 3.354 Å (LLP20), which suggests the expansion of the unit cell volume. However, with the increase of P₂S₅ content, the diffraction peaks of LLP30, LLP40, and LLP50 gradually converts from crystalline to amorphous phase, which are consistent with previous reports in Li₃PS₄ composite SSE (Figure S2, Supporting Information).^[52] As shown in Figure 1c, the Raman spectra of 3LiBH₄-LiI and LLP20 samples were measured between 350 and 2600 cm⁻¹. A broad band at ≈ 2311 cm⁻¹ can be attributed to [BH₄⁻] vibration in the hexagonal high-temperature phase of 3LiBH₄-LiI and LLP20. The shoulder at 2375 cm⁻¹ can be categorized as the stretching band of [BH₄⁻] in different chemical environments. LLP20 samples containing P₂S₅ display a strong band at 420 cm⁻¹, which can be assigned to the vibration of the [PS₄³⁻] ions. Meanwhile, the presence of [PS₄³⁻] is identified by a wide band from 542 to 564 cm⁻¹ owing to the increase of the length of [PS₄³⁻] chains.^[51,53] Furthermore, a minor amount of sulfur unit ion (S₆²⁻ and S₄²⁻) were observed in the spectra at 452 and 488 cm⁻¹, resulting from the decomposition of P₂S₅ by separation of exocyclic sulfur.^[54,55] In general, comprehensive analysis of XRD and Raman experimental results suggests that the BH₄⁻ ions are partially substituted by PS₄³⁻ and I⁻ ions. SEM images of the as-prepared LLP_x powders are shown in Figure S2, Supporting Information. All the SSE powders are a few to tens of μm size with irregular morphology. The microscopic surface of these samples looks very smooth, indicating that the sample has good flexibility during assembly.

3.2. Electrochemical Performance

The ionic conductivity of LLP_x was measured by EIS with Li electrodes. The results of LiBH₄ and 3LiBH₄-LiI as references

were also compared. The Arrhenius plots of LLP_x show a linear increase in the logarithmic values. Among the series samples of LLP_x ($0 \leq x \leq 50$) in Figure 2a, the LLP20 sample shows the highest conductivity at 30 °C, 3.77×10^{-4} S cm⁻¹. Further increasing temperature to 50 and 100 °C, LLP20 exhibits a lithium ionic conductivity of 1.12×10^{-3} and 1.0×10^{-2} S cm⁻¹. The EIS results of LLP20 with blocking electrodes was also measured and shown in Figure S3, Supporting Information. Figure 2b shows the typical Nyquist plots obtained from LLP20. The impedance presents a semicircle during the measure region, which is attributed to the bulk and grain boundary. Their diameters sensitively decrease with increasing temperature from 30 to 100 °C. Correspondingly, the obtained conductivities follow an Arrhenius trend according to the relation:

$$\sigma T = \sigma_0 \exp(-E_a/kT) \quad (1)$$

where σ is the ionic conductivity and E_a is the activation energy. The ionic conductivity and the activation energy were the largest and the lowest for $x = 20$ (Figure 2c). These are σ (100 °C) = 1.0×10^{-2} S cm⁻¹ and 0.49 eV, respectively. This conductivity is comparable to those of hydride-based, oxide-based, sulfide-based, and polymer-based electrolytes (Figure 2d). These results imply a strong possibility on the further investigation of a new generation of solid-state batteries with high-energy density. In this case, the following measurements would focus on the LLP20 sample.

Figure 3a–c show the CV curves of the LLP20 sample as compared with 3LiBH₄-LiI and LLP30. A pair of peaks corresponding to Li plating/stripping (lithium deposition Li⁺+e⁻ → Li, and dissolution Li → Li⁺+e⁻) near 0 V versus Li/Li⁺ was observed, and no additional current response corresponding to electrochemical reactions appeared up to 5 V versus Li/Li⁺, which demonstrated the high electrochemical stability of 3LiBH₄-LiI and LLP20 samples (Figure 3a,b). Notably, the LLP20 electrolyte revealed in a fairly low current peak during Li plating/stripping. However, Figure 3c shows the CV curves of LLP30 sample, which a board peak could be observed from 1 to 3 V. This indicates that the LLP30 electrolyte is unstable under this voltage range. It also suggests that the addition of excessive sulfide leads to the formation of amorphous, which further reduces its electrochemical stability.^[56–58] Furthermore, the electrochemical oxidative stability of LLP20 based on linear sweep voltammetry were measured according to the method reported previously. Proper addition of the conductive carbon and its ratio in the composite electrolytes are important for an accurate determination of the intrinsic oxidative stability. Figure S6, Supporting Information, shows the representative linear sweep voltammograms at 100 $\mu\text{V s}^{-1}$, using Ketjenblack, 5 wt%. The value of E_{onset} was 1.97 V versus Li⁺/Li, attributing to a sufficiently large electronic contact area. This intrinsic electrochemical window is smaller than that without carbon addition (Figure 3b). However, there was no obvious detection of hydride-based electrolyte decomposition and side reactions during discharge–charge process (Figure 4). This is mainly owing to the formation of the stable interface that hinders the side reaction between cathode and electrolyte, which has been proved by previous study.^[59] For example, Orimo and co-workers experimentally observed the formation of Li₂B₁₂H₁₂ as a result of thermal decomposition of

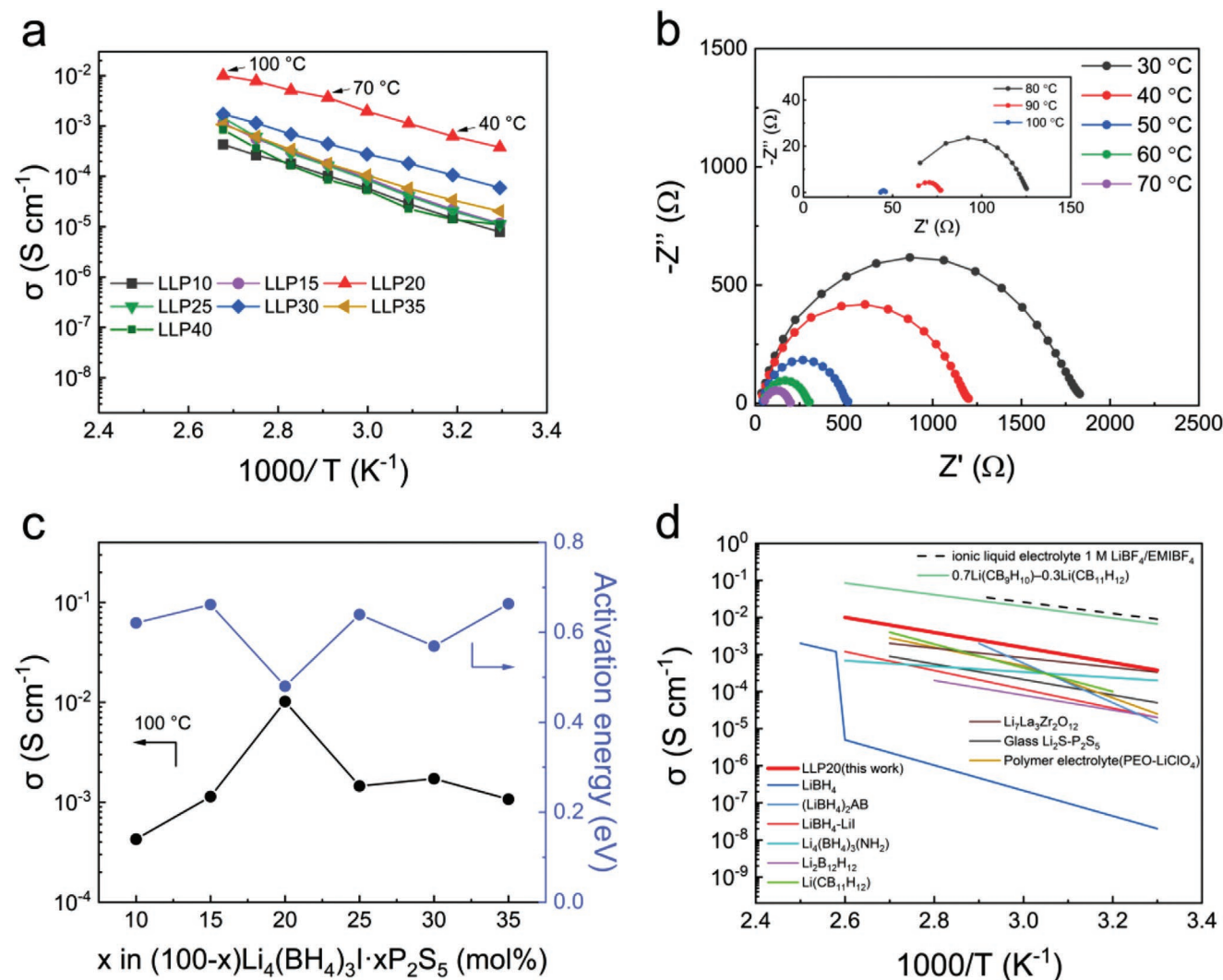


Figure 2. a) Arrhenius ionic conductivity plots of LLPx. b) Typical Nyquist plots of LLP20. c) The ionic conductivity at 100 °C, and the activation energies of LLPx as a function of x. d) Arrhenius ionic conductivity plots of LLP20, LiBH₄-based complex hydride and other types of electrolytes.^[29,40,41,43,46,74–78]

LiBH₄.^[60] Ohba and co-workers have examined the phase relationship of the ternary Li-B-H-hydrides by the first-principles calculations.^[61] The authors suggested that Li₂B₁₂H₁₂ is thermodynamically stable and thereby occurs as an intermediate stable phase between cathode and electrolyte. On the other hand, the corresponding dQ/dV curves were shown in Figure 4f. There is an irreversible electrochemical oxidation wave attributed to the side-reaction appeared in the voltage range around 1.2 V at the 2nd cycle. Such an irreversible electrochemical oxidation was not observed from the 3rd cycle onward, and the coulombic efficiency became almost 100%. These results suggest that the electrolyte and electrode have good stability during discharge and charge cycling.

Then, to evaluate the lithium ion transfer capability across the interface with the lithium metal anode, the Li plating/stripping cycling was measured at 100 °C. When galvanostatically cycled at different current densities from 0.2 to 0.5 mA cm⁻² in both directions for 1 h, the Li/LLP20/Li cell exhibits superior voltage retention and electrochemical stability compared

with Li/3LiBH₄-LiI/Li cell (shortcut at 470 h). The magnified potential curve as shown in Figure 3d, and represents the plated and stripped details between the two electrodes without sudden drop in the overpotential. A very flat potential profile for plating/stripping throughout cycling, which implying the absence of formation of high-surface-area Li microstructures, such as, Li dendrites.^[62] Remarkably, the voltage remains stable over 500 cycles (or 1000 h) compared with other type electrolytes such as, oxide-^[63–67] and sulfide-^[68–70] electrolytes.

The interfaces between the Li metal and SSEs after 500 cycles were observed by cross-sectional SEM in Figure 3f. Compared with fresh Li metal (Figure 3g), an obvious interface area of newly formed Li around 15 μm thick without needle-like Li dendrite was found after long time cycling. No apparent cracks are observed in cross-section of electrolytes near the interface area, which corresponds to Zhang et al. and Sun et al.'s research that electrolytes with the high Li⁺ transference number lead to a uniform diffusion and stable deposition of Li⁺, further suppressing the formation of Li dendrites at the interface of

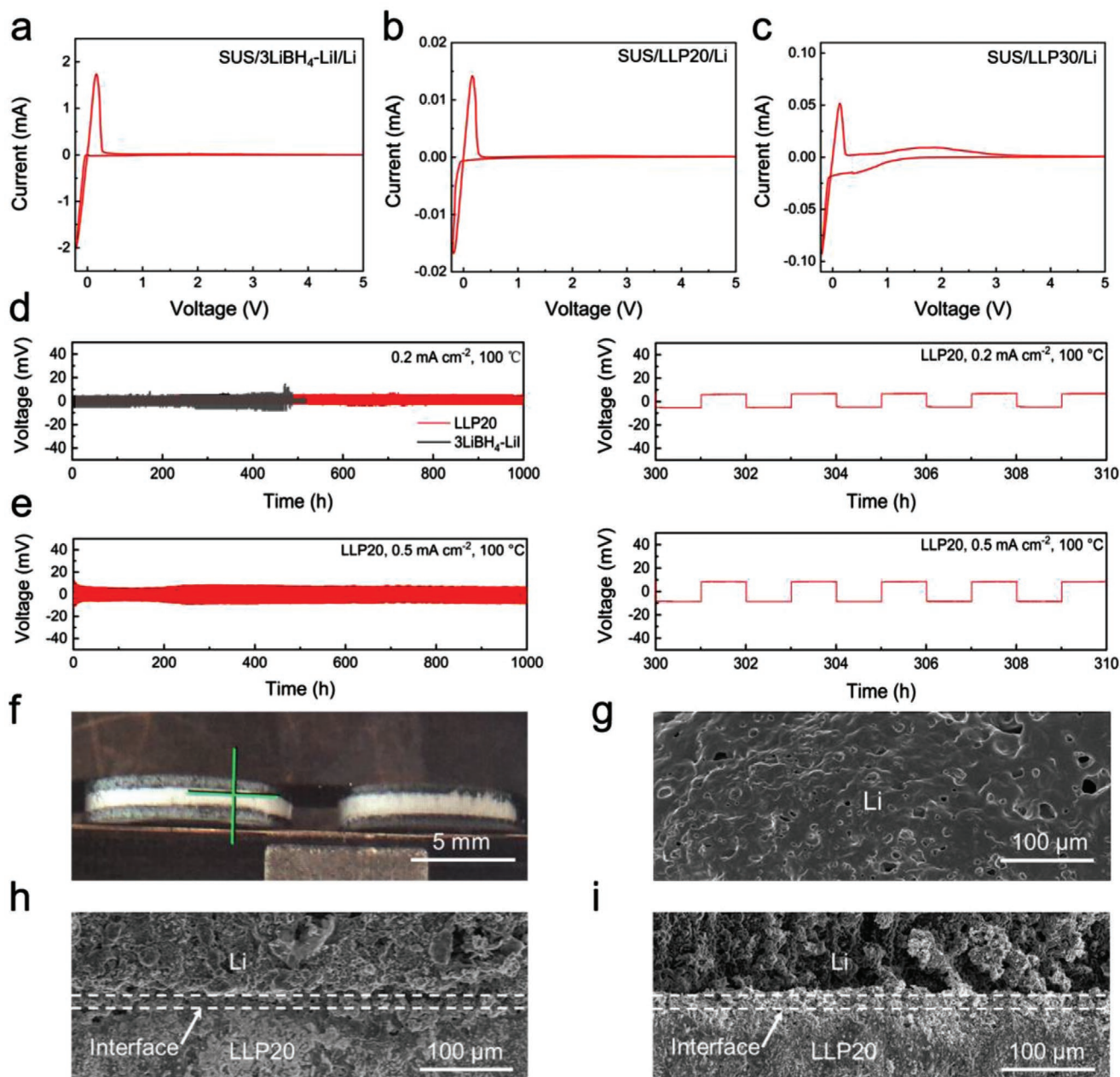


Figure 3. Cyclic voltammogram (CV) operated in an asymmetric cell at 100 °C and a scan rate of 5 mV s⁻¹ of a) SUS/3LiBH₄-Li/Li, b) SUS/LLP20/Li, and c) SUS/LLP30/Li, respectively. Galvanostatic cycling curves of Li/LLP20/Li symmetric cells. Voltage transients during Li plating/stripping with different current densities at 100 °C d) 0.2 mA cm⁻², e) 0.5 mA cm⁻². SEM image of the LLP20/Li interface. f) Cross section of digital photo. g) Fresh Li. h) Current density at 0.2 mA cm⁻² after 500 cycles, and i) current density at 0.5 mA cm⁻² after 500 cycles.

Li/SSE.^[71-73] However, as shown in Figure S4, Supporting Information, cracks are observed inside the LLP20 SSE upon long time cycling, which indicates the place of origin for nucleation of Li dendrites. This is also consistent with the short-circuit mechanism of LiBH₄-based SSEs. Moreover, Figure S5a, Supporting Information, shows the voltage profiles with stepped current density. Obviously, a sudden decrease in the overpotential occurred at 1.6 mA cm⁻², probably owing to the Li dendrite formation. To investigate the durability of the interface against fast charging and discharging, a Li plating/stripping test was

conducted under a current density of 1.0 mA cm⁻² as shown in Figure S5b, Supporting Information. The symmetric cell showed an excellent stability even after 1000 h also certifies that the composite SSEs can maintain their stability against Li metal and exhibit high compatibility with Li metal, which is very suitable as a potential SSE.

The direct current (DC) conductivity of LLP20 was measured by using lithium electrodes and SUS electrodes. The DC conductivity of LLP20 for lithium electrodes (SUS electrodes) was determined around 4.1 × 10⁻⁴ S cm⁻¹ (3.1 × 10⁻¹⁰ S cm⁻¹, 40 °C),

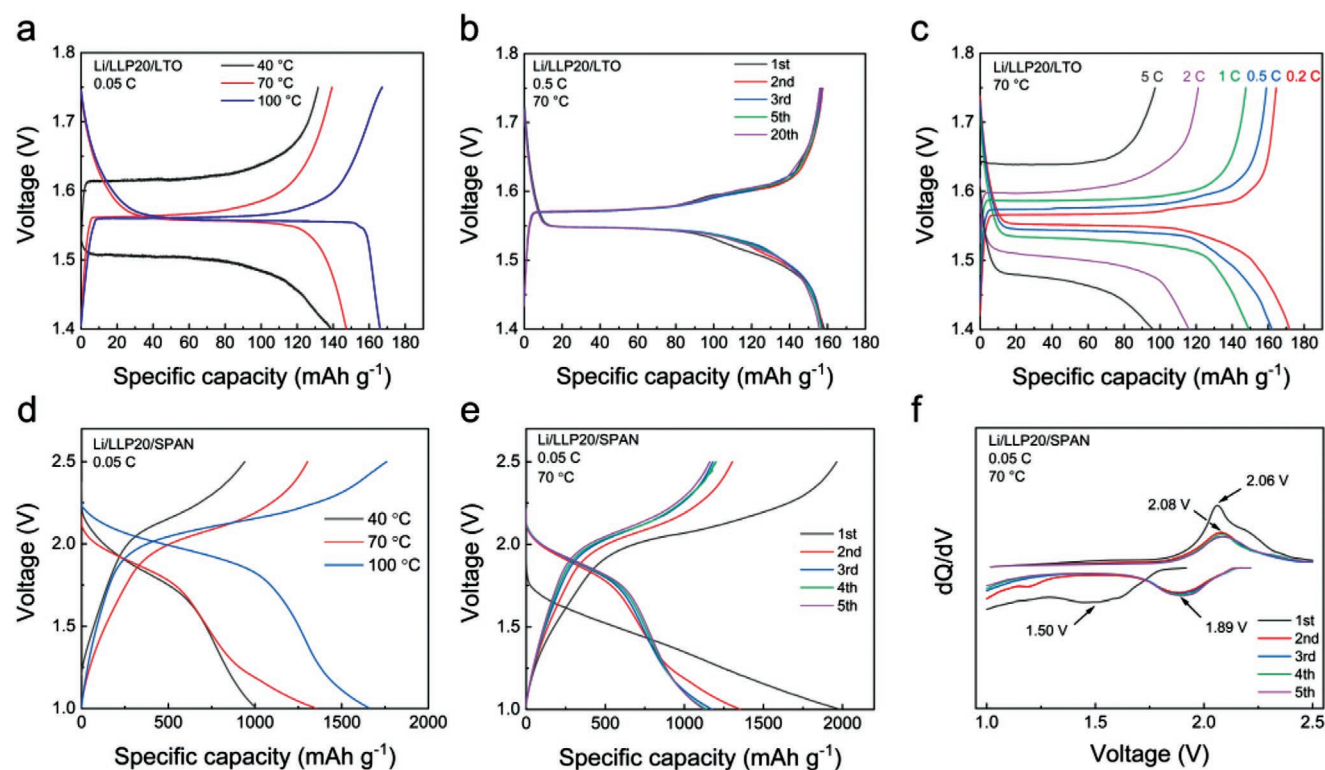


Figure 4. a) Charge–discharge profiles of Li/LLP20/LTO at 40, 70, and 100 °C. b) Cycling performance of Li/LLP20/LTO at 70 °C. c) Rate performance at 0.2, 0.5, 1, 2, and 5 C at 70 °C. d) Charge–discharge profiles of Li/LLP20/SPAN at 40, 70, and 100 °C. e) Cycling performance of Li/LLP20/SPAN at 70 °C. f) Differential capacitance curves of galvanostatic cycling curves in (e).

$1.9 \times 10^{-3} \text{ S cm}^{-1}$ ($1.4 \times 10^{-9} \text{ S cm}^{-1}$, 70 °C), and $5.7 \times 10^{-3} \text{ S cm}^{-1}$ ($1.2 \times 10^{-8} \text{ S cm}^{-1}$, 100 °C) after 1000 s, respectively, which are at least 5 orders of magnitude higher than that for SUS electrodes (Figure S7, Supporting Information). Furthermore, the EIS impedance of Li/Li cell and Li/SPAN cell were measured before and after cycling. A very flat potential profile for plating/stripping throughout cycling and the resistance of cell has no obvious increase after cycling (Figure S8, Supporting Information). These DC values of lithium electrodes agree with the EIS results, indicating that no distinct impedance of interface exists between electrode and electrolyte. Accordingly, the lithium ion transference number (t_c) for LLP20 was calculated based on the equation below:

$$t_c = 1 - D_{\text{SUS}}/D_{\text{Li}} \quad (2)$$

where D_{SUS} and D_{Li} are the DC conductivities, respectively. The t_c for LLP20 are almost same at different temperature, 0.9999, which means the Li^+ contributes independently to the charge transference and the electronic conduction is almost negligible in this study.

3.3. All Solid-State Batteries Performance

Herein, to demonstrate the adequacy of the LLP20 composite electrolyte for all-solid-state batteries, two types of all-solid-state batteries, Li/LLP20/ $\text{Li}_4\text{Ti}_5\text{O}_{12}$ (LTO) and Li/LLP20/SPAN,

were assembled and cycling tested. Figure 4a,d shows the charge/discharge curves at 40, 70, and 100 °C, respectively. The corresponding discharge capacities for LTO are 138, 147, and 166 mAh g^{-1} , and for SPAN are 1009, 1354, and 1662 mAh g^{-1} at a current density of 0.05 C, indicating a wide temperature application for LLP20. The charge/discharge tests were measured at 0.5 C and 70 °C as shown in Figure 4b. The initial discharge capacity is 158 mAh g^{-1} , which is equivalent to 90% of the theoretical capacity for LTO (175 mAh g^{-1}). The discharged capacity can be relatively well-maintained (up to 156 mAh g^{-1}) after 20 cycles. More importantly, 100% of the coulombic efficiency can be retained during cycling. As shown in Figure 4c, the cell exhibits good rate performance with specific capacities of 171, 162, 149, 116, and 96 mA h g^{-1} at 0.2, 0.5, 1, 2, and 5 C, respectively. Meanwhile, for SPAN electrode, cycling performance of Li/LLP20/SPAN full cell was tested at the current density of 0.05 C for sulfur as active material in the voltage range from 1.0 to 2.5 V (vs Li/Li⁺). The corresponding discharge–charge curves were shown in Figure 4e (dQ/dV curves in Figure 4f). The discharge capacity and charge capacity were 1354 and 1303 mAh g^{-1} in the second cycle (96% S utilization), respectively. The cycling performance was also tested at 40 and 100 °C as shown in Figures S8 and S9, Supporting Information. The discharged capacity can be well-maintained even after 100 cycles, certifying the excellent performance of LLP20 as SSE. The above preliminary results strongly prove that LLP20 is a promising electrolyte material. The overall performance of all solid-state batteries using LLP20 can be further improved

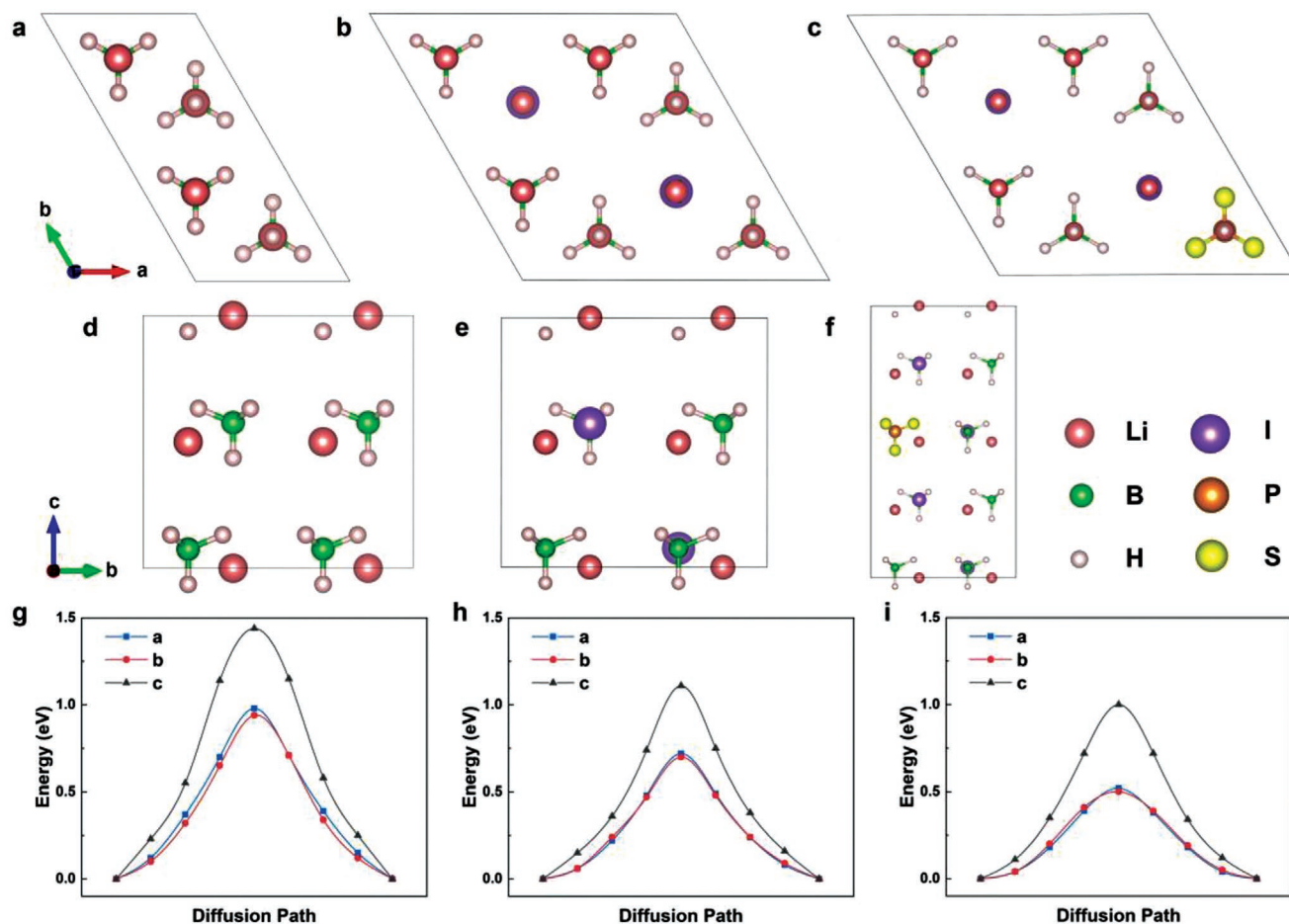


Figure 5. Schematic calculation models of a) LiBH_4 , b) $\text{LiBH}_4\text{-LiI}$, c) LLP20 from c-axis, and d) LiBH_4 , e) $\text{LiBH}_4\text{-LiI}$, f) LLP20 from a-axis; g,h,i) Li ion diffusion barriers along a, b, and c axes in LiBH_4 , $\text{LiBH}_4\text{-LiI}$, and LLP20, respectively.

through electrode optimization and interface modification, which will be completed in our future work.

3.4. Lithium Ion Diffusion Mechanism

To further investigate the mechanism of Li^+ diffusion and the high ion conductivity in LLP20, first-principal calculations using nudged elastic band method were carried out by studying the diffusion pathways and barriers in LiBH_4 , $3\text{LiBH}_4\text{-LiI}$, and LLP20. According to experimental data, a $2 \times 1 \times 1$ supercell of LiBH_4 was used to simulate Li^+ diffusion in pure LiBH_4 (Figure 5a,d); two BH_4 group replaced by two I atoms was set in a $2 \times 2 \times 1$ supercell of LiBH_4 to form the $3\text{LiBH}_4\text{-LiI}$ lattice (Figure 5b,e); a $2 \times 2 \times 2$ supercell of LiBH_4 based on $3\text{LiBH}_4\text{-LiI}$ was used to simulate LLPx in which a BH_4 group was replaced by PS_4 group (Figure 5c,f). Figure 5g–i show the Li^+ diffusion barriers along with the diffusion pathways in three axes directions. As shown in Figure 5g, Li^+ could diffuse along a and b axes with much lower barriers (0.98 and 0.94 eV) than along c axis (1.44 eV) in pure LiBH_4 , which may result from the space barrier of BH_4 group in the Li ion diffusion pathway along c axis. In Figure 5h,i, the similar phenomenon could also be observed both in $3\text{LiBH}_4\text{-LiI}$ and LLPx, in which

the diffusion barriers along c axis are about 50% higher than those along a or b axis. Furthermore, after doping with I ions in LiBH_4 , Li^+ is easier to diffuse in a or b axis (about 0.70 eV) than in pure LiBH_4 (about 0.95 eV). When PS_4 group is induced into $3\text{LiBH}_4\text{-LiI}$, the diffusion barrier in a or b axis further decreased to 0.50 eV. Because the dopants of I ions and PS_4 group have larger volume than BH_4 group, inducing larger lattice volumes in $3\text{LiBH}_4\text{-LiI}$ and LLPx, the higher ion conductivity could be attributed to the larger space in lattice and lower diffusion barrier. As a result, LLPx has a small Li^+ concentration (9.55 nm^{-3}), compared with LiBH_4 (18.35 nm^{-3}) and $3\text{LiBH}_4\text{-LiI}$ (11.63 nm^{-3}). Therefore, the doping with I ion and PS_4 group could enhance the ion conductivity of LiBH_4 by decreasing Li ion diffusion barrier, providing further evidence of the fast ion migration in LLPx.

4. Conclusions

In summary, a series of composite SSEs consisted of hydride and sulfide was developed in this study. After P_2S_5 doped, no phase transition was observed. The concept of double anions substitution has been verified, which help successfully stabilize the high temperature phase in room temperature. A

preliminary study reveals the high reorientational mobility associated with the anions could assist the high lithium ionic conductivity. Thereby a high lithium ionic conductivity of $2.3 \times 10^{-4} \text{ S cm}^{-1}$ was realized at $30 \text{ }^\circ\text{C}$ with a wide electrochemical window of 0–5 V. Notably, the instantaneous voltage remains stable over 500 cycles (or 1000 h) under a current density of 1.0 mA cm^{-2} . The composite SSEs can maintain their stability against Li metal and exhibit high compatibility with Li metal. Moreover, all solid-state batteries were assembled and tested in a wide temperature range, which presented notable cyclability and reversibility. These results could provide principles for exploring high-performance composite SSEs from single SSEs and contribute to the development of next-generation LIBs with high energy density.

Supporting Information

Supporting Information is available from the Wiley Online Library or from the author.

Acknowledgements

T.Z. and X.Y. acknowledge support from the National Natural Science Foundation of China (51625102, 51802154). X.Y. acknowledges support from Open Fund of Jiangsu Key Laboratory of Electrochemical Energy Storage Technologies No. EEST2019-2. The authors would like to thank Prof. Hujun Cao (Dalian Institute of Chemical Physics, Chinese Academy of Sciences), Prof. Teng He (Dalian Institute of Chemical Physics, Chinese Academy of Sciences), Prof. Quanqun Pang (Peking University), Prof. Junhao Lin (Southern University of Science and Technology, China), and Prof. Wei Zhang (Southeast University) for their kind help and useful discussion in this work.

Conflict of Interest

The authors declare no conflict of interest.

Author Contributions

T.Z. and X.Y. conceived and designed the experiments. All the authors contributed to the experiment and data analysis. P.L. contributed to the first-principles calculation. T.Z., Y.H., G.X., and X.Y. contributed to the Raman and SEM analysis. X.Y. provided valuable feedback and supported the electrochemical analysis. All the authors contributed to manuscript writing.

Data Availability Statement

Research data are not shared.

Keywords

complex hydrides, LiBH_4 , lithium ionic conductivity, solid-state electrolytes, sulfide electrolytes

Received: June 7, 2021
Published online: July 9, 2021

- [1] N. Zhao, W. Khokhar, Z. Bi, C. Shi, X. Guo, L. Z. Fan, C. W. Nan, *Joule* **2019**, *3*, 1190.
- [2] X. B. Cheng, C. Z. Zhao, Y. X. Yao, H. Liu, Q. Zhang, *Chem* **2019**, *5*, 74.
- [3] A. Miura, N. C. Rosero-Navarro, A. Sakuda, K. Tadanaga, N. H. H. Phuc, A. Matsuda, N. Machida, A. Hayashi, M. Tatsumisago, *Nat. Rev. Chem.* **2019**, *3*, 189.
- [4] Y. Gao, Z. Yan, J. L. Gray, X. He, D. Wang, T. Chen, Q. Huang, Y. C. Li, H. Wang, S. H. Kim, T. E. Mallouk, D. Wang, *Nat. Mater.* **2019**, *18*, 384.
- [5] Z. Gao, H. Sun, L. Fu, F. Ye, Y. Zhang, W. Luo, Y. Huang, *Adv. Mater.* **2018**, *30*, 1705702.
- [6] F. Han, J. Yue, C. Chen, N. Zhao, X. Fan, Z. Ma, T. Gao, F. Wang, X. Guo, C. Wang, *Joule* **2018**, *2*, 497.
- [7] A. Manthiram, X. Yu, S. Wang, *Nat. Rev. Mater.* **2017**, *2*, 16103.
- [8] T. Zhang, Y. Wang, T. Song, H. Miyaoka, K. Shinzato, H. Miyaoka, T. Ichikawa, S. Shi, X. Zhang, S. Isobe, N. Hashimoto, Y. Kojima, *Joule* **2018**, *2*, 1522.
- [9] T. Zhang, W. He, W. Zhang, T. Wang, P. Li, Z. Sun, X. Yu, *Chem. Sci.* **2020**, *11*, 8686.
- [10] Y. X. Song, Y. Shi, J. Wan, S. Y. Lang, X. C. Hu, H. J. Yan, B. Liu, Y. G. Guo, R. Wen, L. J. Wan, *Energy Environ. Sci.* **2019**, *12*, 2496.
- [11] J. Wan, J. Xie, X. Kong, Z. Liu, K. Liu, F. Shi, A. Pei, H. Chen, W. Chen, J. Chen, X. Zhang, L. Zong, J. Wang, L. Q. Chen, J. Qin, Y. Cui, *Nat. Nanotechnol.* **2019**, *14*, 705.
- [12] Y. Kato, S. Hori, T. Saito, K. Suzuki, M. Hirayama, A. Mitsui, M. Yonemura, H. Iba, R. Kanno, *Nat. Energy* **2016**, *1*, 16030.
- [13] Z. Liu, W. Fu, E. A. Payzant, X. Yu, Z. Wu, N. J. Dudney, J. Kiggans, K. Hong, A. J. Rondinone, C. Liang, *J. Am. Chem. Soc.* **2013**, *135*, 975.
- [14] J. B. Goodenough, K. S. Park, *J. Am. Chem. Soc.* **2013**, *135*, 1167.
- [15] E. Quartarone, P. Mustarelli, *Chem. Soc. Rev.* **2011**, *40*, 2525.
- [16] B. Dunn, H. Kamath, J. M. Tarascon, *Science* **2011**, *334*, 928.
- [17] X. Yu, *J. Electrochem. Soc.* **1997**, *144*, 524.
- [18] F. Zheng, M. Kotobuki, S. Song, M. O. Lai, L. Lu, *J. Power Sources* **2018**, *389*, 198.
- [19] Y. Meesala, A. Jena, H. Chang, R. S. Liu, *ACS Energy Lett.* **2017**, *2*, 2734.
- [20] C. Ma, K. Chen, C. Liang, C. W. Nan, R. Ishikawa, K. More, M. Chi, *Energy Environ. Sci.* **2014**, *7*, 1638.
- [21] Y. Inaguma, C. Lique, M. Itoh, T. Nakamura, T. Uchida, H. Ikuta, M. Wakihara, *Solid State Commun.* **1993**, *86*, 689.
- [22] J. Płcharski, W. Weiczorek, *Solid State Ionics* **1988**, *28–30*, 979.
- [23] B. E. Francisco, C. R. Stoldt, J. C. M'Peko, *Chem. Mater.* **2014**, *26*, 4741.
- [24] S. D. Lee, K. N. Jung, H. Kim, H. S. Shin, S. W. Song, M. S. Park, J. W. Lee, *ChemSusChem* **2017**, *10*, 2175.
- [25] S. Ramakumar, C. Deviannapoorani, L. Dhivya, L. S. Shankar, R. Murugan, *Prog. Mater. Sci.* **2017**, *88*, 325.
- [26] L. Chen, Y. Li, S. P. Li, L. Z. Fan, C. W. Nan, J. B. Goodenough, *Nano Energy* **2018**, *46*, 176.
- [27] J. Zheng, M. Tang, Y.-Y. Hu, *Angew. Chem., Int. Ed.* **2016**, *55*, 12538.
- [28] X. He, Y. Zhu, Y. Mo, *Nat. Commun.* **2017**, *8*, 15893.
- [29] R. Murugan, V. Thangadurai, W. Weppner, *Angew. Chem., Int. Ed.* **2007**, *46*, 7778.
- [30] H. Muramatsu, A. Hayashi, T. Ohtomo, S. Hama, M. Tatsumisago, *Solid State Ionics* **2011**, *182*, 116.
- [31] K. H. Park, Q. Bai, D. H. Kim, D. Y. Oh, Y. Zhu, Y. Mo, Y. S. Jung, *Adv. Energy Mater.* **2018**, *8*, 1800035.
- [32] A. Hayashi, H. Muramatsu, T. Ohtomo, S. Hama, M. Tatsumisago, *J. Mater. Chem. A* **2013**, *1*, 6320.
- [33] T. Asano, A. Sakai, S. Ouchi, M. Sakaida, A. Miyazaki, S. Hasegawa, *Adv. Mater.* **2018**, *30*, 1803075.
- [34] X. Li, J. Liang, N. Chen, J. Luo, K. R. Adair, C. Wang, M. N. Banis, T. Sham, L. Zhang, S. Zhao, S. Lu, H. Huang, R. Li, X. Sun, *Angew. Chem., Int. Ed.* **2019**, *131*, 16579.

- [35] R. Mohtadi, *Chem* **2018**, *4*, 1770.
- [36] S. Kim, H. Oguchi, N. Toyama, T. Sato, S. Takagi, T. Otomo, D. Arunkumar, N. Kuwata, J. Kawamura, S. Orimo, *Nat. Commun.* **2019**, *10*, 1081.
- [37] F. Lu, Y. Pang, M. Zhu, F. Han, J. Yang, F. Fang, D. Sun, S. Zheng, C. Wang, *Adv. Funct. Mater.* **2019**, *29*, 1809219.
- [38] M. Matsuo, S. Orimo, *Adv. Energy Mater.* **2011**, *1*, 161.
- [39] T. Zhang, S. Isobe, M. Matsuo, S. Orimo, Y. Wang, N. Hashimoto, S. Ohnuki, *ACS Catal.* **2015**, *5*, 1552.
- [40] M. Matsuo, A. Remhof, P. Martelli, R. Caputo, M. Ernst, Y. Miura, T. Sato, H. Oguchi, H. Maekawa, H. Takamura, A. Borgschulte, A. Züttel, S. I. Orimo, *J. Am. Chem. Soc.* **2009**, *131*, 16389.
- [41] A. Unemoto, M. Matsuo, S. Orimo, *Adv. Funct. Mater.* **2014**, *24*, 2267.
- [42] W. S. Tang, M. Matsuo, H. Wu, V. Stavila, W. Zhou, A. A. Talin, A. V. Soloninin, R. V. Skoryunov, O. A. Babanova, A. V. Skripov, A. Unemoto, S.-I. Orimo, T. J. Udovic, *Adv. Energy Mater.* **2016**, *6*, 1502237.
- [43] M. Matsuo, Y. Nakamori, S. I. Orimo, H. Maekawa, H. Takamura, *Appl. Phys. Lett.* **2007**, *91*, 224103.
- [44] R. Mohtadi, S. Orimo, *Nat. Rev. Mater.* **2017**, *2*, 16091.
- [45] X. Zhang, T. Zhang, Y. Shao, H. Cao, Z. Liu, S. Wang, X. Zhang, *ACS Sustainable Chem. Eng.* **2021**, *9*, 5396.
- [46] H. Maekawa, M. Matsuo, H. Takamura, M. Ando, Y. Noda, T. Karahashi, S. Orimo, *J. Am. Chem. Soc.* **2009**, *131*, 894.
- [47] L. Zhan, Y. Zhang, X. Zhuang, H. Fang, Y. Zhu, X. Guo, J. Chen, Z. Wang, L. Li, *Solid State Ionics* **2017**, *304*, 150.
- [48] A. Hayashi, A. Sakuda, M. Tatsumisago, *Front. Energy Res.* **2016**, *4*, 25.
- [49] Y. Zhu, X. He, Y. Mo, *ACS Appl. Mater. Interfaces* **2015**, *7*, 23685.
- [50] H. Zhai, P. Xu, M. Ning, Q. Cheng, J. Mandal, Y. Yang, *Nano Lett.* **2017**, *17*, 3182.
- [51] A. El Kharbachi, J. Wind, A. Ruud, A. B. Høgset, M. M. Nygård, J. Zhang, M. H. Sørby, S. Kim, F. Cuevas, S. I. Orimo, M. Fichtner, M. Latroche, H. Fjellvåg, B. C. Hauback, *Phys. Chem. Chem. Phys.* **2020**, *22*, 13872.
- [52] A. Yamauchi, A. Sakuda, A. Hayashi, M. Tatsumisago, *J. Power Sources* **2013**, *244*, 707.
- [53] A. El kharbachi, Y. Hu, K. Yoshida, P. Vajeeston, S. Kim, M. H. Sørby, S. Orimo, H. Fjellvåg, B. C. Hauback, *Electrochim. Acta* **2018**, *278*, 332.
- [54] H. Stöffler, T. Zinkevich, M. Yavuz, A. L. Hansen, M. Knapp, J. Bednarčík, S. Randau, F. H. Richter, J. Janek, H. Ehrenberg, S. Indris, *J. Phys. Chem. C* **2019**, *123*, 10280.
- [55] M. Somer, W. Bues, W. Brückner, *Z. Naturforsch., A: Phys. Sci.* **1983**, *38*, 163.
- [56] S. Ujiiie, A. Hayashi, M. Tatsumisago, *Solid State Ionics* **2012**, *211*, 42.
- [57] R. Mercier, J. P. Malugani, B. Fahys, G. Robert, *Solid State Ionics* **1981**, *5*, 663.
- [58] K. Takada, S. Nakano, T. Inada, A. Kajiyama, H. Sasaki, S. Kondo, M. Watanabe, *J. Electrochem. Soc.* **2003**, *150*, A274.
- [59] Z. Lu, F. Ciucci, *Chem. Mater.* **2017**, *29*, 9308.
- [60] A. Unemoto, T. Ikeshoji, S. Yasaku, M. Matsuo, V. Stavila, T. J. Udovic, S.-I. Orimo, *Chem. Mater.* **2015**, *27*, 5407.
- [61] N. Ohba, K. Miwa, M. Aoki, T. Noritake, S. I. Towata, Y. Nakamori, S. I. Orimo, A. Züttel, *Phys. Rev. B: Condens. Matter Mater. Phys.* **2006**, *74*, 075110.
- [62] Q. Pang, X. Liang, A. Shyamsunder, L. F. Nazar, *Joule* **2017**, *1*, 871.
- [63] K. Fu, Y. Gong, B. Liu, Y. Zhu, S. Xu, Y. Yao, W. Luo, C. Wang, S. D. Lacey, J. Dai, Y. Chen, Y. Mo, E. Wachsman, L. Hu, *Sci. Adv.* **2017**, *3*, e1601659.
- [64] Y. Shao, H. Wang, Z. Gong, D. Wang, B. Zheng, J. Zhu, Y. Lu, Y. S. Hu, X. Guo, H. Li, X. Huang, Y. Yang, C. W. Nan, L. Chen, *ACS Energy Lett.* **2018**, *3*, 1212.
- [65] Y. Shen, Y. Zhang, S. Han, J. Wang, Z. Peng, L. Chen, *Joule* **2018**, *2*, 1674.
- [66] B. Liu, Y. Gong, K. Fu, X. Han, Y. Yao, G. Pastel, C. Yang, H. Xie, E. D. Wachsman, L. Hu, *ACS Appl. Mater. Interfaces* **2017**, *9*, 18809.
- [67] A. Jena, Y. Meesala, S. F. Hu, H. Chang, R. S. Liu, *ACS Energy Lett.* **2018**, *3*, 2775.
- [68] W. D. Richards, L. J. Miara, Y. Wang, J. C. Kim, G. Ceder, *Chem. Mater.* **2016**, *28*, 266.
- [69] Z. D. Hood, H. Wang, Y. Li, A. S. Pandian, M. Parans Paranthaman, C. Liang, *Solid State Ionics* **2015**, *283*, 75.
- [70] Q. Zhang, D. Cao, Y. Ma, A. Natan, P. Aurora, H. Zhu, *Adv. Mater.* **2019**, *31*, 1901131.
- [71] F. Mo, J. Ruan, S. Sun, Z. Lian, S. Yang, X. Yue, Y. Song, Y. Zhou, F. Fang, G. Sun, S. Peng, D. Sun, *Adv. Energy Mater.* **2019**, *9*, 1902123.
- [72] Z. Zou, Y. Li, Z. Lu, D. Wang, Y. Cui, B. Guo, Y. Li, X. Liang, J. Feng, H. Li, C. W. Nan, M. Armand, L. Chen, K. Xu, S. Shi, *Chem. Rev.* **2020**, *120*, 4169.
- [73] L. Chen, W. Li, L. Fan, C. Nan, Q. Zhang, *Adv. Funct. Mater.* **2019**, *29*, 1901047.
- [74] M. Pan, C. Feng, Q. Wang, L. Zhang, Q. Chao, *J. Cent. South Univ. Technol.* **2007**, *14*, 348.
- [75] M. Matsuo, S. I. Orimo, *Adv. Energy Mater.* **2011**, *1*, 161.
- [76] F. Mizuno, A. Hayashi, K. Tadanaga, M. Tatsumisago, *Adv. Mater.* **2005**, *17*, 918.
- [77] H. Liu, Z. Ren, X. Zhang, J. Hu, M. Gao, H. Pan, Y. Liu, *Chem. Mater.* **2020**, *32*, 671.
- [78] W. S. Tang, A. Unemoto, W. Zhou, V. Stavila, M. Matsuo, H. Wu, S.-I. Orimo, T. J. Udovic, *Energy Environ. Sci.* **2015**, *8*, 3637.